Determination of the boundary temperature errors by variation of two temperature sensor locations in a one-dimensional inverse heat conduction problem

Received January 1996
Revised January 1997

Tzu-Fang Chen, Sui Lin and Joseph C.Y. Wang
Department of Mechanical Engineering, Concordia University, Montréal, Québec, Canada

Nomenclature

a_1 = coefficient of the linear temperature function, equation (20)
b_1, b_2 = coefficients of the quadratic temperature function, equation (21)
c_1, c_2 = coefficients of the exponential temperature function, equation (22)
d_1, d_2, ω = coefficients of the periodic temperature function, equation (23)
S_- = backward shift operator
S_+ = forward shift operator
t = dimensionless time
T = dimensionless temperature
U = correlation matrix for $n\Delta t$ and $(n + 1)\Delta t$ time levels
x = dimensionless space co-ordinate
χ_L = left hand sensor location (Figure 1)
χ_L^* = left hand specified sensor location
χ_M = right hand sensor location (Figure 1)
χ_M^* = right hand specified sensor location
χ_N = right hand boundary of computational domain, $\chi_N = 1$ (Figure 1)
σ_{LH} = error of the reconstruction temperature at the left hand boundary (per cent)
σ_{LH}^* = error of the reconstruction temperature at the left hand boundary with two specified sensor locations (per cent)
σ_{RH} = error of the reconstruction temperature at the right hand boundary (per cent)
σ_{RH}^* = error of the reconstruction temperature at the right hand boundary with two specified sensor locations (per cent)
Λ_{LH} = constant coefficient in equation (15)
Λ_{RH} = constant coefficient in equation (16)

Subscripts
i = mesh point location in x direction
L = left hand sensor location in finite difference scheme
M = right hand sensor location in finite difference scheme
N = right hand boundary of computational domain in finite difference scheme
o = left hand boundary in finite difference scheme

Superscript
n = time level

1. Introduction

A space boundary inverse heat conduction problem (IHCP) is a problem that can reconstruct the unknown boundary temperature or boundary heat flux with one or more measured temperatures inside the heat conducting solid. This problem has been widely investigated by many researchers, for example, Beck

The present work is being supported by the National Science and Engineering Research Council of Canada under Grant No. OGP0001681 and Grant No. OGP0007929.

International Journal for Numerical Methods for Heat & Fluid Flow
Vol. 7 No. 7, 1997, pp. 635–646.

et al.[1], Flach and Özişik[2,3], Hsu *et al.*[4], Katz and Rubinsky[5], Kurpisz[6,7], Murio[8], Stolz[9], and others. They have developed different techniques and inverse solvers to solve IHCPs. IHCPs are not the same as the direct heat conduction problems which are "well-posed". The IHCPs are a kind of "ill-posed" problem[1,8]. Due to the property of the iIl-posed problem, it has non-existence, non-uniqueness and instability of the solution[10]. This property has unstable characteristics. Prediction of an unknown boundary temperature by an IHCP is not an easy event. In order to have a reliable estimate of the temperature on the boundary surface, errors caused by the locations of interior temperature sensors will be investigated. This paper considers a one-dimensional IHCP in dimensionless form, which is solved by using a time marching implicit finite difference inverse solver[11], and investigates the errors caused by the variation of two interior sensor locations. Simple error relations have been established from the numerical results of selected boundary functions for estimating the errors of reconstruction temperatures at the both side boundaries.

2. An exact solution used for error prediction of IHCP

In this section, we address the problem of a conducting solid with two interior temperature sensors located at points $x = \chi_L$ (left hand sensor) and $x = \chi_M$ (right hand sensor) as shown in Figure 1. The solid has two dimensionless specified surface at $x = 0$ and $x = \chi_N = 1$. These two sensors are movable between x = 0 and $x = 0$ and $x = \chi_N = 1$ (the left hand boundary and the right hand boundary of the computational domain respectively).

The exact solution of the one-dimensional semi-infinite heat conduction equation in a dimensionless form will be used for comparing the recovery surface temperatures of the numerical results. The errors caused by the change of the two sensor locations are determined by a time marching implicit finite difference scheme.

The dimensionless conduction equation of the semi-infinite solid is expressed by:

$$\frac{\partial T}{\partial t} = \frac{\partial^2 T}{\partial x^2} \tag{1}$$

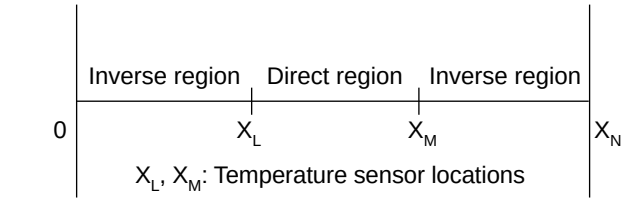

Unknown conditions:
$Q(0, t) = ?$, $Q(X_N, t) = ?$
$T(0, t) = ?$, $T(X_N, t) = ?$

Known conditions:
$T(X_L, t) =$ known
$T(X_M, t) =$ known

Figure 1.
Two sensor locations of the one-dimensional IHCP

with the following initial and boundary conditions,

$$T(x,0) = 0 \tag{2}$$

$$T(0,t) = f(t) \tag{3}$$

$$T(\infty,t) = 0 \tag{4}$$

The exact solution[12] of the system of equations (1) to (4) is:

$$T(x,t) = \frac{2}{\sqrt{\pi}} \int_{\frac{x}{2\sqrt{t}}}^{\infty} f(t - \frac{x^2}{4\mu^2}) e^{-\mu^2} d\mu \tag{5}$$

The IHCP considered in this paper is shown in Figure 1. It is considered that the temperature data at the two interior sensor locations $x = \chi_L$ and $x = \chi_M$ are taken from equation (5). The inverse problem is to find the unknown time histories of the temperatures and heat fluxes at the left hand boundary of the solid $x = 0$ and at the right hand boundary of the computational domain $x = \chi_N = 1$. The numerical reconstruction results at $x = 0$ and $x = \chi_N = 1$ are then compared with those of the exact solution, equation (5), to obtain the error percentages at $x = 0$ and $x = \chi_N = 1$ caused by the change of the sensor locations.

3. Numerical scheme of the IHCP

A fully implicit finite difference scheme of equations (1)-(4) can be written in the form:

$$U\underline{T}^{n+1} = \underline{T}^{n} \tag{6}$$

where U is a matrix with the forward and backward shift operators S_+ and S_-. For example, the finite difference scheme equation (6) is

$$-\lambda T_{i+1}^{n+1} + (1 + 2\lambda) T_i^{n+1} - \lambda T_{i-1}^{n+1} = T_i^n \tag{7}$$

where λ is equal to $\frac{\Delta t}{(\Delta x)^2}$. By using the shift operators S_+ and S_-, equation (7) becomes

$$-\lambda S_+ T_i^{n+1} + (1 + 2\lambda) T_i^{n+1} - \lambda S_- T_i^{n+1} = T_i^n \tag{8}$$

or

$$(-\lambda S_+ + (1 + 2\lambda) - \lambda S_-) T_i^{n+1} = T_i^n \tag{9}$$

where T_i^n are the elements of matrix $\underline{T}^n$.

Applying the left hand boundary heat flux, q_0^{n+1}, at the $(n + 1)\Delta t$ time level to the implicit finite difference solver, equation (7), gives

$$(1 + \lambda) T_o^{n+1} - \lambda T_1^{n+1} + \lambda \Delta x q_o^{n+1} = T_o^n \tag{10}$$

Similarly, applying the right hand boundary heat flux q_N^{n+1} at $(n + 1)\Delta t$ time level to the implicit finite difference solver, equation (7), yields

$$(1+\lambda)\,T_N^{n+1} - \lambda T_{N-1}^{n+1} - \lambda \Delta x q_N^{n+1} = T_N^n \tag{11}$$

For the numerical calculation, equation (6) has to be properly formulated as follows[11]: The temperatures of the two sensors located at points $x = \chi_L$ and $x = \chi_M$ (as shown in Figure 1) at the $(n + 1)\Delta t$ time level, T_L^{n+1} and T_M^{n+1}, are known, which may be added into the positions of T_L^n and T_M^n in the matrix $\underline{T}^n$ of equation(6). The unknown heat fluxes q_0^{n+1} and q_N^{n+1} at the both hand boundaries may be substituted into the positions of the elements T_L^{n+1} and T_M^{n+1} in the matrix $\underline{T}^{n+1}$ of equation(6). The two boundary heat flux coefficients, $+\lambda\Delta x$ for q_0^{n+1} and $-\lambda\Delta x$ for q_N^{n+1}, may be substituted into the corresponding element positions in the correlation U matrix of the equation(6).

The matrix U of equation (6) is expressed by:

$$U = \begin{bmatrix}
1+\lambda & -\lambda & 0 & \dots & 0 & 0 & \lambda\Delta x & 0 & 0 & \dots & 0 & & & 0 \\
 & & & & \cdot & \cdot & \cdot & & & & & & & \\
 & & & & -\lambda & 1+2\lambda & 0 & & & & & & & \\
 & & & & & -\lambda & 0 & \lambda & & & & & & \\
 & & & & & & 0 & 1+2\lambda & -\lambda & & & & & \\
 & & & & & & & \cdot & \cdot & \cdot & & & & \\
 & & & & & & & & -\lambda & 1+2\lambda & 0 & & & \\
 & & & & & & & & & -\lambda & 0 & -\lambda & & \\
 & & & & & & \cdot & & & & 0 & 1+2\lambda & -\lambda & \\
 & & & & & & & & & & \cdot & \cdot & \cdot & \\
0 & & & & & & 0 & & & \dots & -\lambda\Delta x & \dots & -\lambda & 1+\lambda
\end{bmatrix} \tag{12}$$

The unknown matrix of $\underline{T}^{n+1}$ equation (6) can be written as:

$$\underline{T}^{n+1} = \begin{bmatrix}
T_o^{n+1} \\
\cdot \\
T_{L-1}^{n+1} \\
q_o^{n+1} \\
T_{L+1}^{n+1} \\
\cdot \\
T_{M-1}^{n+1} \\
q_N^{n+1} \\
T_{M+1}^{n+1} \\
\cdot \\
T_N^{n+1}
\end{bmatrix} \tag{13}$$

The matrix $\underline{T}^n$ of equation (6) has the form:

$$\underline{T}^n = \begin{bmatrix} T_o^n \\ \cdot \\ T_{L-1}^n + \lambda T_L^{n+1} \\ T_L^n - (2\lambda+1)T_L^{n+1} \\ T_{L+1}^n + \lambda T_L^n \\ \cdot \\ T_{M-1}^n + \lambda T_M^{n+1} \\ T_M^n - (2\lambda+1)T_M^{n+1} \\ T_{M+1}^n + \lambda T_M^{n+1} \\ \cdot \\ T_N^n \end{bmatrix} \tag{14}$$

Then the unknowns of the matrix $\underline{T}^{n+1}$, including reconstruction temperatures and heat fluxes at the boundary $x = 0$ and $x = 1$, can be solved by the time marching scheme.

4. Numerical experiments

Numerical simulation results indicate that the errors of the reconstruction temperature at the left and right hand boundaries can be simplified by the following relations:

- At the left hand boundary, $x = 0$,

$$\sigma_{LH}(\%) = \Lambda_{LH} \cdot \chi_L \cdot \chi_M \tag{15}$$

- At the right hand boundary of the computational domain, $x = 1$,

$$\sigma_{RH}(\%) = \Lambda_{RH} \cdot (1 - \chi_L) \cdot (1 - \chi_M) \tag{16}$$

where

$$0 < \chi_L < \chi_M < 1 \tag{17}$$

The coefficients Λ_{LH} and Λ_{RH} can be determined by using one numerical simulation through the inverse solver of a pair of specified sensor locations at $x = \chi_L^*$ and $x = \chi_M^*$ to obtain σ_{LH}^* and σ_{RH}^*. Owing to the ill-posed condition of the inverse problem, the distance between the two sensor locations at $x = \chi_L^*$ and $x = \chi_M^*$ should be taken as far as possible[13]. In the present study, the distance between the two sensor locations should not be taken shorter than 0.05 in the dimensionless scale, i.e. $|\chi_L^* - \chi_M^*| \geq 0.05$.

The coefficients, Λ_{LH} and Λ_{RH}, can then be determined from equations (15)-(16) as follows,

$$\Lambda_{LH} = \frac{\sigma_{LH}^*}{\chi_L^* \cdot \chi_M^*} \tag{18}$$

$$\Lambda_{RH} = \frac{\sigma^*_{RH}}{(1-\chi^*_L)\cdot(1-\chi^*_M)} \tag{19}$$

To confirm the error relations presented in equations (15)-(16), the following four temperature functions for the boundary condition $f(t)$ appearing in equation (3) will be used.

- *Case 1*: A linear function ($a_1 > 0$)

$$f(t) = a_1 t \tag{20}$$

- *Case 2*: A quadratic function ($b_1 \geq 0$, $b_2 > 0$)

$$f(t) = b_1 t + b_2 t^2 \tag{21}$$

- *Case 3*: An exponential function ($c_1 > 0$, $c_2 > 0$)

$$f(t) = c_1 e^{c_2 t} \tag{22}$$

- *Case 4*: A periodic function ($d_1 > 0$, $d_2 > 0$, $\omega > 0$)

$$f(t) = d_1 + d_2 \sin(\omega \cdot t) \tag{23}$$

To determine the coefficients Λ_{LH} and Λ_{RH}, numerical values of a_1, b_1, b_2, c_1, c_2, d_1, d_2, and ω appearing in equations (20) to (23) have to be fixed. With the mesh size $\Delta x = 0.05$, $\Delta t = 0.05$, the selected parameter values of the functions and the calculated results of σ^*_{LH}, σ^*_{RH}, Λ^*_{LH}, Λ^*_{RH}, and two specified sensor locations are summarized as follows,

- *Case 1*: A linear function

$$a_1 = 50 \quad ; \quad \chi^*_L = 0.35 \quad ; \quad \sigma^*_{LH} = 1.070 \quad ; \quad \Lambda_{LH} = 4.703$$
$$\chi^*_M = 0.65 \qquad \sigma^*_{RH} = 1.218 \qquad \Lambda_{RH} = 5.354$$

The recovery errors at the left and right hand boundaries, from equations (15) and (16), are:

$$\sigma_{LH}(\%) = 4.703 \cdot \chi_L \cdot \chi_M \tag{24}$$

$$\sigma_{RH}(\%) = 5.354 \cdot (1-\chi_L)\cdot(1-\chi_M) \tag{25}$$

- *Case 2*: A quadratic function

$$b_1 = 50 \quad ; \quad \chi^*_L = 0.35 \quad ; \quad \sigma^*_{LH} = 1.373 \quad ; \quad \Lambda_{LH} = 6.035$$
$$b_2 = 2 \qquad \chi^*_M = 0.65 \qquad \sigma^*_{RH} = 1.563 \qquad \Lambda_{RH} = 6.870$$

The recovery errors at the left and right hand boundaries, from equations (15) and (16), are:

$$\sigma_{LH}(\%) = 6.035 \cdot \chi_L \cdot \chi_M \tag{26}$$

$$\sigma_{RH}(\%) = 6.870 \cdot (1-\chi_L)\cdot(1-\chi_M) \tag{27}$$

- *Case 3*: An exponential function

$$c_1 = 50 \quad ; \quad \chi_L^* = 0.35 \quad ; \quad \sigma_{LH}^* = 2.649 \quad ; \quad \Lambda_{LH} = 11.644$$
$$c_2 = 2 \qquad \chi_M^* = 0.65 \qquad \sigma_{RH}^* = 3.015 \qquad \Lambda_{RH} = 13.252$$

The recovery errors at the left and right hand side boundaries, from equations (15) and (16), are:

$$\sigma_{LH}(\%) = 11.644 \cdot \chi_L \cdot \chi_M \tag{28}$$

$$\sigma_{RH}(\%) = 13.252 \cdot (1 - \chi_L) \cdot (1 - \chi_M) \tag{29}$$

- *Case 4*: A periodic function

$$d_1 = 150 \quad ; \quad \chi_L^* = 0.35 \quad ; \quad \sigma_{LH}^* = 2.868 \quad ; \quad \Lambda_{LH} = 12.606$$
$$d_2 = 40 \qquad \chi_M^* = 0.65 \qquad \sigma_{RH}^* = 3.264 \qquad \Lambda_{RH} = 14.347$$
$$\omega = 2.5$$

The recovery errors at the left and right hand side boundaries, from equations (15) and (16), are:

$$\sigma_{LH}(\%) = 12.606 \cdot \chi_L \cdot \chi_M \tag{30}$$

$$\sigma_{RH}(\%) = 14.347 \cdot (1 - \chi_L) \cdot (1 - \chi_M) \tag{31}$$

Figures 2-9 illustrate the following. Figures 2, 4, 6 and 8 show that the errors of the reconstruction temperature at the left hand boundary, $x = 0$, as a function of the right hand sensor location with the left hand sensor location as a parameter for cases 1 to 4 respectively. Similarly, Figures 3, 5, 7 and 9 show that the errors

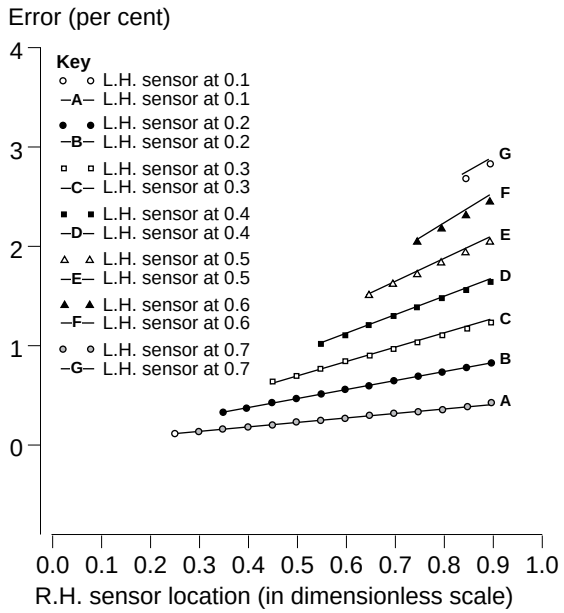

Figure 2. Error of the reconstruction temperature at the L.H. boundary as a function of the R.H. sensor location for case 1 with the L.H. sensor location as parameter

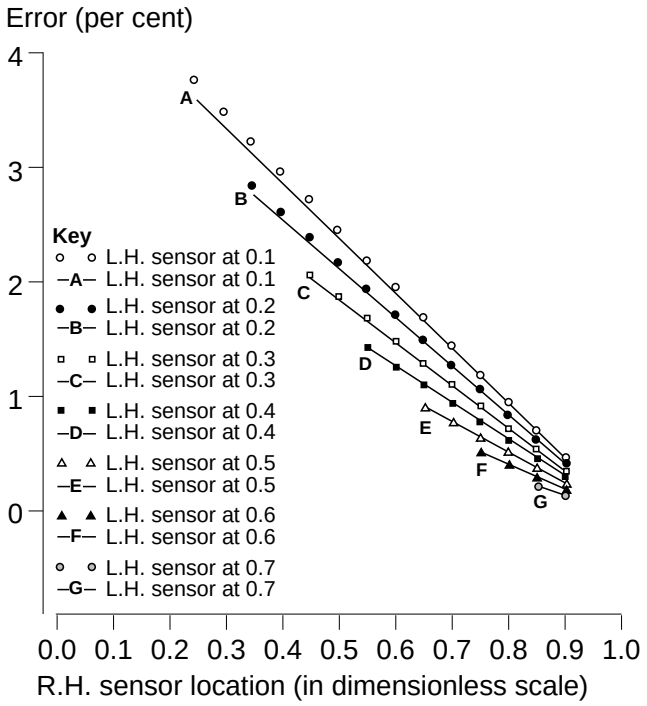

Figure 3.
Error of the reconstruction temperature at the R.H. boundary as a function of the R.H. sensor location for case 1 with the L.H. sensor location as parameter

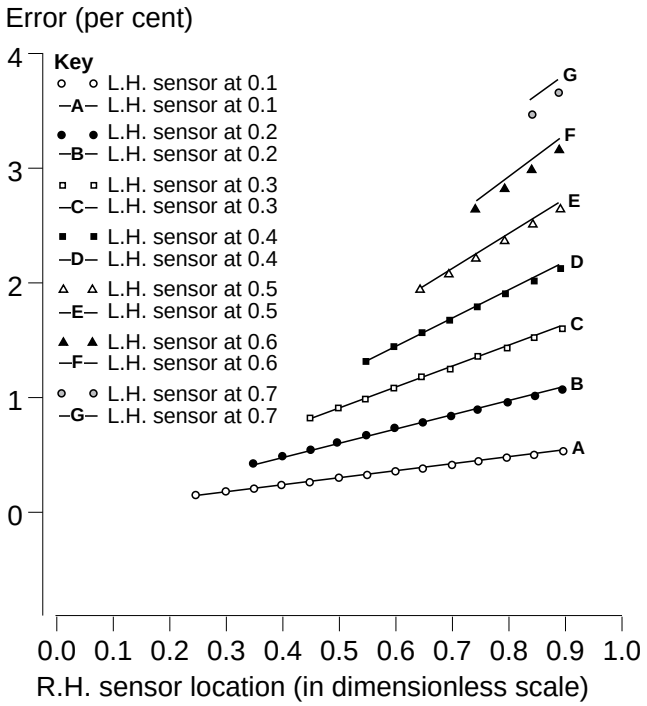

Figure 4.
Error of the reconstruction temperature at the L.H. boundary as a function of the R.H. sensor location for case 2 with the L.H. sensor location as parameter

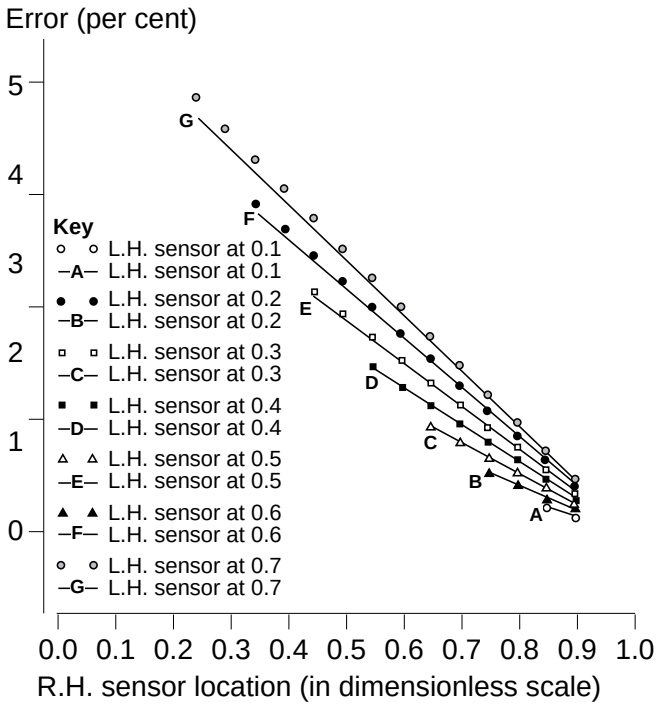

Figure 5. Error of the reconstruction temperature at the R.H. boundary as a function of the R.H. sensor location for case 2 with the L.H. sensor location as parameter

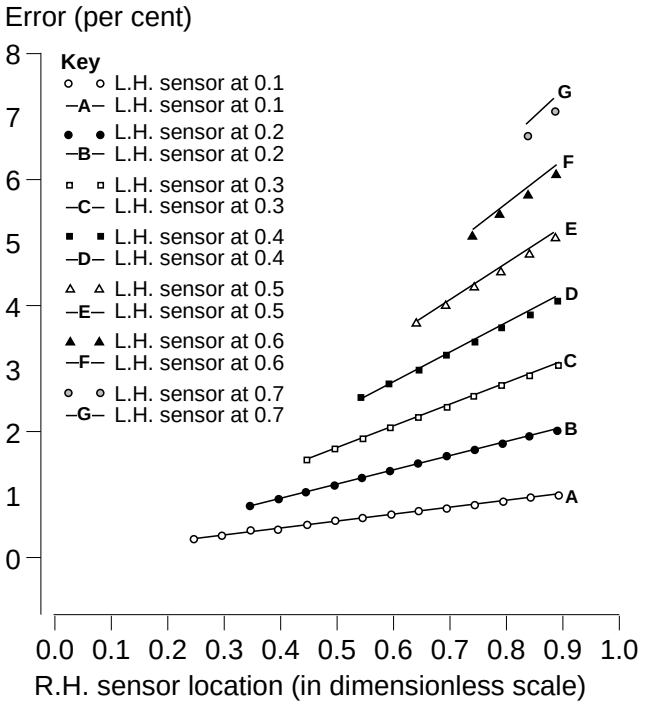

Figure 6. Error of the reconstruction temperature at the L.H. boundary as a function of the R.H. sensor location for case 3 with the L.H. sensor location as parameter

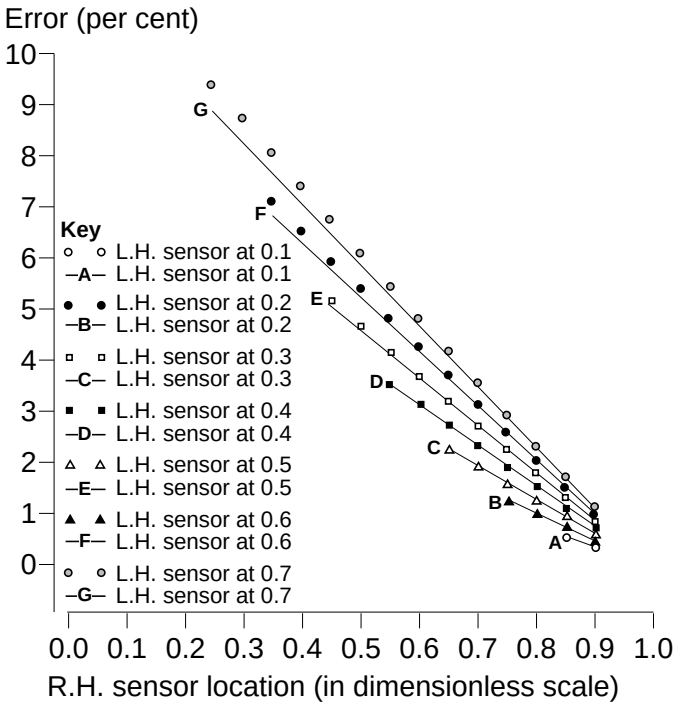

Figure 7.
Error of the reconstruction temperature at the R.H. boundary as a function of the R.H. sensor location for case 3 with the L.H. sensor location as parameter

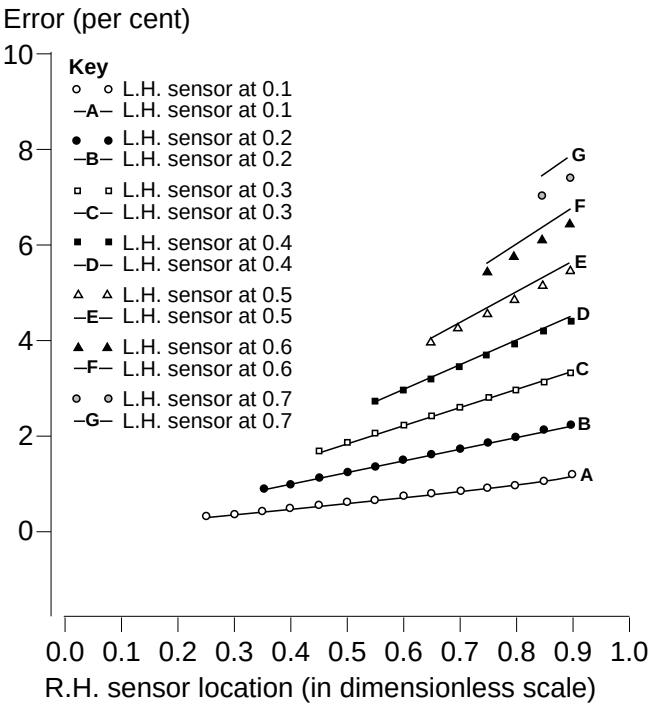

Figure 8.
Error of the reconstruction temperature at the L.H. boundary as a function of the R.H. sensor location for case 4 with the L.H. sensor location as parameter

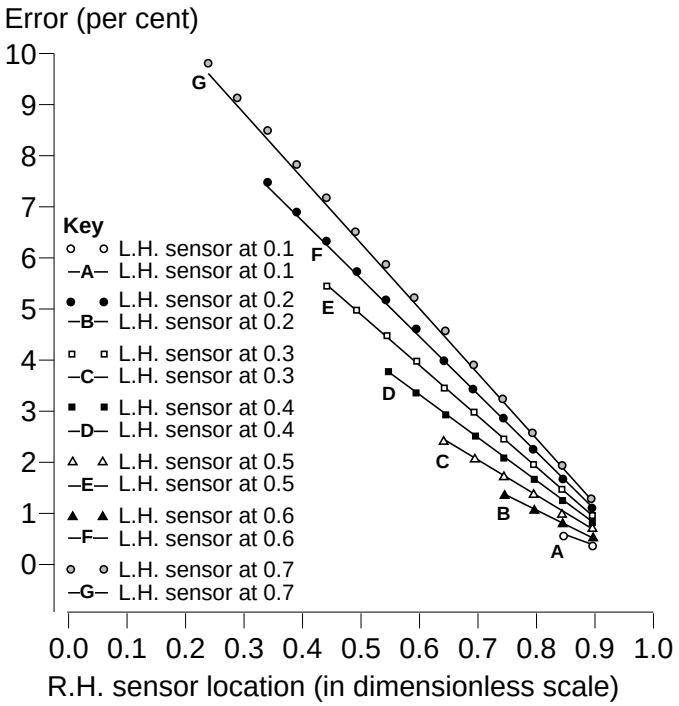

Figure 9. Error of the reconstruction temperature at the R.H. boundary as a function of the R.H. sensor location for case 4 with the L.H. sensor location as parameter

of the reconstruction temperature at the right hand boundary, $x = \chi_N = 1$, as a function of the right hand sensor location with the left hand sensor location as a parameter for cases 1 to 4 respectively. The symbols and lines appearing in Figures 2 to 9 are the values calculated by the inverse solver presented in section 3, and by the simplified relations, equations (24) to (31) respectively. The differences between the results obtained from the simplified relations, equations (24) to (31), and the results calculated by the inverse solver are very small, within a relative error of 0.5 per cent.

5. Conclusions

From the numerical calculation the following conclusions can be drawn:

(1) The errors of the reconstruction temperature at the left and right hand boundaries, caused by the variation of the two sensors located in $0 < \chi_L < \chi_M < 1$ of a one-dimensional IHCP, can be approximately determined by the simple relations, equations (15) and (16) respectively.

(2) Equations (15) and (16) are confirmed by the selected four temperature functions, equations (20) to (23). The characteristics of the errors of the reconstruction temperatures are summarized by the numerical simulation as follows:

- Case 1, the linear function, equation (20):
  Equations (24) and (25) are available for any positive value of a_1 in equation (20).
- Cases 2 and 3, the quadratic and exponential functions, equations (21) and (22), respectively:
  For cases 2 and 3, the larger the temperature slope, $\frac{df(t)}{dt}$, at $x = 0$, the larger the errors of the reconstruction temperatures at the both side boundaries.
- Case 4, the periodic function, equation (23):
  For a given value of ω in the range of $0 < \omega < 5$ in equation (23), the larger the ratio of the coefficients $\frac{d_2}{d_1}$, the larger the errors of the reconstruction temperatures at the both side boundaries.

(3) The numerical results show that the effect of time on the errors of the reconstruction temperature is negligibly small.

References

1. Beck, J.V., Blackwell, B. and St Clair, C.R. Jr, *Inverse Heat Conduction*, John Wiley & Sons, New York, NY, 1985.
2. Flach, G.P. and Özişik, M.N., "Inverse heat conduction problem of simultaneously estimating spatially varying thermal conductivity and heat capacity per unit volume", *Numer. Heat Transfer*, Part A, Vol. 16, 1989, pp. 441-61.
3. Flach, G.P. and Özişik, M.N., "An adaptive inverse heat conduction method with automatic control", *ASME J. Heat Transfer*, Vol. 114, 1992, pp. 5-13.
4. Hsu, T.R., Sun, N.S., Chen, G.G. and Gong, Z.L., "Finite element formulation for two-dimensional inverse heat conduction analysis", *ASME J. Heat Transfer*, Vol. 114, 1992, pp. 553-7.
5. Katz, M.A. and Rubinsky, B., "An inverse finite-element technique to determine the change of phase interface location in one-dimensional melting problems", *Numer. Heat Transfer*, Vol. 7, 1984, pp. 269-83.
6. Kurpisz, K., "Numerical solution of one case of inverse heat conduction problems", *ASME J. Heat Transfer*, Vol. 113, 1991, pp. 280-6.
7. Kurpisz, K. and Nowak, A.J., *Inverse Thermal Problems*, Computational Mechanics Publications, Southampton, 1995.
8. Murio, D.A., *The Mollification Method and Numerical Solution of Ill-posed Problem*, John Wiley & Sons, New York, NY, 1993.
9. Stolz, G. Jr, "Numerical solutions to an inverse problem of heat conduction for simple shapes", *ASME J. Heat Transfer*, Vol. 82, 1960, pp. 20-6.
10. Hadamard, J., *Lectures on Cauchy's Problem in Linear Partial Difference Equations*, Yale University Press, New Howen, CT.
11. Chen, T.-F., Lin, S. and Wang, J.C.Y., "Kalman filter and finite difference scheme to inverse heat conduction problems", *Inverse Problems in Engineering*, Vol. 3, 1996, pp. 162-75.
12. Carslaw, H.S. and Jaeger, J.C., *Conduction of Heat in Solid*, Oxford University Press, Oxford, 1959.
13. Hensel, E., *Inverse Theory and Applications for Engineers*, Prentice-Hall, Englewood Cliffs, NJ, 1991.